Unidirectional emissions from dielectric photonic circuits decorated with plasmonic phased antenna arrays*

Ding Wei(丁 伟)†, Chen Yu-Hui(陈宇辉), and Li Zhi-Yuan(李志远)

Laboratory of Optical Physics, Institute of Physics, Chinese Academy of Sciences, Beijing 100190, *China*

(Received 7 October 2013; revised manuscript received 7 November 2013; published online 24 January 2014)

Thanks to resonant characteristics of metallic nanoparticles, optical waves scattered from plasmonic nanoantennae can be well tailored in both amplitude and phase. We numerically demonstrate that, by varying the lengths and the lateral positions of gold nanorods in vicinity of a silicon waveguide, unidirectional emissions with typical forward–backward contrast ratio of 15 dB and directivity of 12 dB can be acquired in a plasmonic phased antenna array with sub-wavelength device length. The properties, i.e., the emission directionality and the size compactness, can be employed to control the far-field radiation pattern from a dielectric photonic circuit. Moreover, by altering the orientations of the dielectric waveguides decorated with plasmonic phased antenna arrays, we propose wireless light transportations in a layered photonic infrastructure, which may have applications in high-density photonic integrations.

Keywords: surface plasmons, optical properties of nanoparticles, optical structures, light scattering

PACS: 73.20.Mf, 78.67.Bf, 78.67.–n, 42.25.Fx **DOI:** 10.1088/1674-1056/23/3/037301

1. Introduction

Localized surface plasmons are collective excitations of the conduction electrons in metallic nanostructures coupled to the electromagnetic field.[1] Last fifteen years have witnessed continuously increasing activities in exploiting the near-field enhancement and localization properties of the surface plasmon resonators to favor nanometer-scale light–material interactions,[2–5] and to miniaturize optical circuits.[6,7] In the meantime, by utilizing the far-field properties of the surface plasmon resonators, people have also explored the applications of optical nanoantennae,[8–12] which convert energy from localized electromagnetic emitters to directionally propagating waves with very small footprints.[13–17] The effects of the surface plasmon resonators are embodied in the field enhancement, localization, and directionality.

Borrowing the idea of Yagi-Uda antenna, which is well known in radio-frequency area[18] Curto *et al.*[16] and Kosako *et al.*[17] have experimentally exhibited unidirectional emissions from optical array antennae. The excitation sources in these two experiments are both localized emitters, which first excite one element of the antenna, i.e., the driven element, and then drag the parasitic elements, i.e., the reflectors and the directors, via mutual coupling between elements. The phase coherence built up in the whole array antenna enforces directional emissions. However, if the antenna lies on an interface between two media, the far-field (FF) term of the mutual coupling, which is inversely proportional to the distance ($\sim 1/r$), disappears at grazing angles.[19] The remainder nearfield (NF) and intermediatefield (IF) terms of the mutual coupling, which are inversely proportional to the cube ($\sim 1/r^3$) and square ($\sim 1/r^2$) of the distance respectively, can only support the nearest-neighbor interactions.[20] Under such circumstances, adding one layer of high-index medium onto the interface, like Ref. [21] does, creates a slab of waveguide and revives the FF inter-element coupling via the guided wave of the slab. Altogether, in order to produce a well-performed Yagi-Uda antenna on a dielectric interface, people need to carefully design the complicated mutual couplings between antenna elements.

On the other hand, if one deliberately suppresses the inter-element couplings and excites all the elements equivalently, unidirectional emissions can also be acquired in a much simpler structure, i.e., the phased antenna array, where the amplitude of the radiated field from each element needs to be equal, and the phase needs to be evenly arranged. Simultaneously fulfilling these two conditions requires utilizing dispersive properties of a resonant antenna. In addition, an extended (rather than a localized) excitation source and a non-enhanced antenna response (so that a lower charge concentration) favor this mechanism. The former guarantees equal excitation strengths for all the elements, and the latter ensures a weak NF/IF inter-element coupling. Note that the FF inter-element coupling is absent at grazing angles.

By either adjusting geometries of metallic nanoparticles[13,14] or altering composite materials of elements,[15] people have demonstrated emission directionality of phased antenna arrays by using plasmonic resonators in the visible wavelength region. Recently, Yu *et al.*[22] and Shadrivov *et al.*[23] employed this concept in so-called

*Project supported by the National Basic Research Program of China (Grant No. 2013CB632704), the National Natural Science Foundation of China (Grant Nos. 11204366 and 61275044), and the Science Foundation of Chinese Academy of Sciences (Grant No. Y1K501DL11).

†Corresponding author. E-mail: wding@iphy.ac.cn

© 2014 Chinese Physical Society and IOP Publishing Ltd

meta-surfaces in the middle-infrared and the GHz frequency regions respectively, where the excited charge densities inside antennae, hence the strength of the NF/IF inter-element couplings, are even weaker. Whether in visible[13–15] or in infrared range,[22,23] the phased antenna arrays are illuminated by plane waves and the vanishment of the inter-element coupling makes the design of this device much easier than Yagi-Uda array antennae.

In this work, we incorporate phased antenna arrays into a dielectric photonic circuit at near-infrared wavelengths, a very useful architecture for telecommunication applications.[24] The guided wave of the dielectric waveguide acts as the extended excitation source, and the quasi-plasmonic characters of the gold nanorods in the telecom wavelength region guarantee the weak NF/IF inter-element couplings. Different from Ref. [21], our gold nanorods are laid laterally aside, not on the top of the dielectric waveguide, which not only eliminates the FF inter-element coupling mediated by the guided wave but also introduces one more geometrical parameter in the process of designing antenna elements to bypass the amplitude/phase dependency. Because of this independent amplitude/phase tunability of the plasmonic nanorods, light emissions from a subwavelength dielectric waveguide can be dramatically engineered.

This paper is organized as follows. Section 2 analyzes the resonant characteristics and the emission properties of a gold nanorod pair excited by a dielectric waveguide. The tunability of the amplitude and phase of the radiated field are numerically calculated. An interference technique is then applied to compose a unidirectional phased antenna array. Section 3 shows the flexible control of the direction and the polarization of the far-field radiation from a dielectric photonic circuit decorated with plasmonic phased antenna arrays. Potential applications of these photonic circuits in wireless light transportations[25] are proposed. The last section ends with discussion and conclusions.

2. Gold nanorod arrays excited by a silicon waveguide

Figure 1(a) depicts a silicon waveguide with the cross section of $w \times h$ lying upon a silica substrate. The superstrate is air. When two identical gold nanorods with the cross section of 80 nm×80 nm symmetrically lie on the two sides of this waveguide, the evanescent field of the guided wave is scattered to the far field. The nanorods act as the antenna device, which converts the guided wave to propagating photons. In Fig. 1(a), the length of the nanorod and the side-to-side separation distance from the nanorod to the waveguide are denoted as l and s, respectively; the direction of the scattered wave is defined according to its tilting angle θ with respect to the normal direction and the azimuthal angle ϕ with respect to the propagating direction of the guided wave. The refractive indices of silicon and silica are 3.475 and 1.444 respectively, and are both assumed to be dispersiveless. The dielectric constants of gold are fitted by a Drude–Lorentz formula based on the experimental data in Ref. [26].

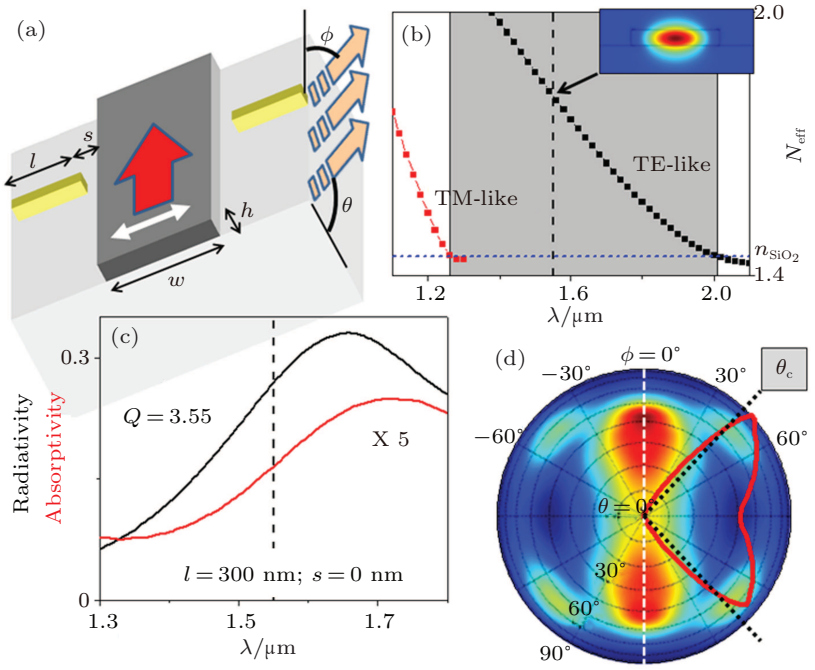


Fig. 1. (color online) (a) Schematic of light radiations (orange arrows) from a pair of Au nanorods in vicinity of a Si waveguide. Geometrical parameters are noted in the diagram. The white and the red arrows represent the field polarization and the direction of the light propagation, respectively. (b) Modal indexes of the TE-like (black) and TM-like (red) guided waves versus the wavelength. Insert: intensity profile of the TE-like mode at the working wavelength $\lambda = 1.55$ μm. FDTD simulated (c) radiativity/absorptivity spectra and (d) radiation pattern of the device in (a). The red curve in (c) is magnified by five for clarity. The red line in (d) is the cut of the radiation pattern along $\phi = 0°/180°$ (the white dashed line), which is presented in a polar coordinate.

2.1. Single-mode waveguides and plasmonic antennae

In order to avoid multi-mode plagues, our studies are carried out in single-mode wavelength range of the waveguide. Under such circumstance, the forward-propagating guided wave can only be scattered into the backward fundamental guided wave or the far-field radiations, besides being absorbed. In this work, we fix the cross section of the silicon waveguide to be 610 nm×105 nm, which gives rise to a single-mode wavelength range spanning 750 nm around the working wavelength $\lambda = 1.55$ μm (see Fig. 1(b)). Three-dimensional (3D) finite-difference time-domain (FDTD) simulations are implemented with the smallest mesh size of 5 nm.

Figure 1(c) plots the simulated spectra of radiativity and absorptivity within the single-mode wavelength range with $l = 300$ nm and $s = 0$ nm. In simulations, we collect the transmitted and reflected powers in the waveguide. The power fluxes flowing into the antennae are also integrated. The radiativity is derived from the supplementary of the transmittivity by deducting the reflectivity and the absorptivity. One can see that the peak wavelength of the radiativity spectrum (the black line) is slightly shorter than that of the absorptivity spectrum (the red line). In Ref. [27], this blue-shift has been interpreted by the relevancy between the radiation (absorption) peak and the enhancement of the oscillatory current (charge) densities inside metallic nanoparticles, where the densities of the oscillatory current, j, and charge ρ obey the conservation condition, $\nabla \cdot j + \partial\rho/\partial t = 0$. From the derived relationship, $j(\lambda)/l \approx \omega \cdot \rho \propto \rho(\lambda)/\lambda$, the peaks of the oscillatory current and charge densities appear at slightly different wavelengths. Figure 1(c) also gives the Q factor of the resonance by dividing the resonant wavelength of the radiation spectrum to the bandwidth at half maximum intensity. Larger Q factor results in more sensitive tunability of the radiated field, which will be discussed later on.

Besides resonant properties, another important index of the plasmonic antenna is its cost–effectiveness ratio, defined as the absorptivity divided by the radiativity. The dissipation-induced thermal problem may become an important challenge for future large-scale photonic integrations.[28] From Fig. 1(c), this index is measured to be ∼1/8 at the working wavelength. In near-infrared range, the relatively small imaginary part of the dielectric constant of gold gives rise to a modest cost–effectiveness ratio. However, this index is indeed influenced by geometries of nanoparticles. According to our simulations of various antenna geometries (data not shown), the cost–effectiveness ratio increases as the cross section of the nanorod shrinks or as the ends of the nanorod are rounded. In both cases, the more serious skin-depth effect, i.e., the overlap of the electric fields with the metal material causes the stronger dissipation. In this work, we adopt the nanorods having flat facets and the cross section of 80 nm×80 nm.

From the FDTD simulations, we also obtain the radiation pattern in the substrate side, $|\boldsymbol{E}|^2/\max(|\boldsymbol{E}|^2)$. As shown in Fig. 1(d) for $l = 300$ nm and $s = 0$ nm, more than 70% of the total radiation goes into the substrate, the radiation profile (the red curve) along the cut line ($\phi = 0°$) is nearly symmetric, and two peaks appear at the critical angle of $\theta_c = \sin^{-1}(1/n_{SiO_2})$. All the features are typical for a non-retardant dipole transversely lying on a dielectric interface.[16,19,29,30]

Recording the radiated field in the normal direction ($\theta = 0°$), figure 2(a) plots its intensity (square of the amplitude) and phase as functions of the antenna length l. The separation distance from the waveguide to the nanorod, s, is set to be zero. In Fig. 2(a), the peak radiation occurs at $l = 290$ nm, and the phase of the radiated field varies in a wide range of about 90°. These two variations originate from the resonant nature of the plasmonic antenna and can be utilized to compose a phased antenna array. In contrast, if the antenna material is replaced by silicon (see Fig. 2(b)), these resonant features disappear in a pure capacitive atmosphere. Here, the plasmonic and non-plasmonic nanoparticles are respectively analog to the inductor and capacitor elements in a picture of nanocircuits.[31]

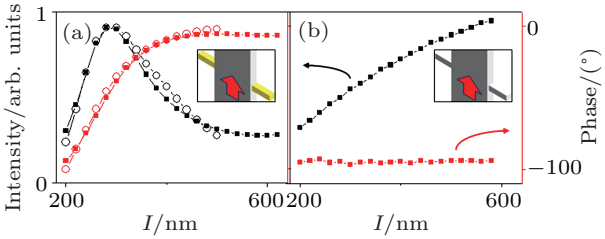


Fig. 2. (color online) FDTD simulated intensities (black squares) and phases (red squares) of the radiations in the normal direction for (a) an Au nanorod pair and (b) a Si nanorod pair excited by a silicon waveguide versus the nanorod length, l. Here, $s = 0$ nm. The white circles in (a) are from Eqs. (1).

The results of the radiations in the normal direction (see Fig. 2(a)) can also be crossly compared with the spectra shown in Fig. 1(c), which represents the spectral dispersions of the gold nanorod pairs from the viewpoint of the guided wave. Once having known the resonant wavelengths (λ_0) and the peak intensities (I_0) of the radiativity spectra, e.g., Fig. 1(c) of different nanorod pairs, the intensity (I) and the phase (φ) of the radiated field in the normal direction can be derived according to the Q factor,[32]

$$I \propto I_0 \frac{\lambda_0^2}{\lambda_0^2 + 4Q^2(\lambda - \lambda_0)^2}, \tag{1a}$$

$$\varphi = \text{atan}\left(2Q\frac{\lambda_0 - \lambda}{\lambda_0}\right). \tag{1b}$$

In Fig. 2(a), the Q factor (equal to 3.55, from Fig. 1(c)) is used, and the agreement between the simulation and Eq. (1) implies that the Q factor of the nanorod antenna determines the tunability of the radiated field. Non-resonant antennae as shown in Fig. 2(b) do not exhibit phase tunability.

Constituting a phased antenna array requires independent control of the amplitude and phase of the radiated field from each element.[22] In our case, it is achieved by adjusting the length (l) and the separation (s) of the nanorods. Figure 3 plots the simulated intensities (a, c) and phases (b, d) of the radiated fields in the directions of ($\theta = 45°$, $\phi = 0°$) (a, b) and ($\theta = 45°$, $\phi = 180°$) (c, d) as functions of l and s. In Ref. [22], similar jobs have been done by sweeping the arm length and the angle of a V-shaped rod antenna in a cross polarization configuration.

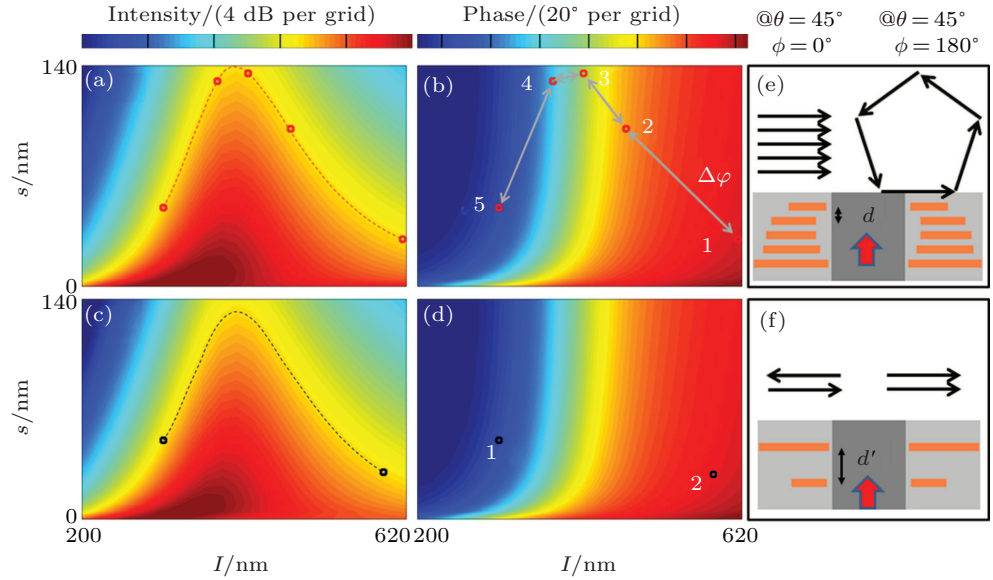


Fig. 3. (color online) Simulated (a, c) intensities and (b, d) phases of the radiated fields in the directions of ($\theta = 45°$, $\phi = 0°$) (a, b) and ($\theta = 45°$, $\phi = 180°$) (c, d) as functions of the nanorod length (l) and the antenna-to- waveguide separation (s). The color scales used in (a, c) and in (b, d) are identical respectively. The red (black) circles in (a,b) ((c, d)) represent five (two) nanorod pairs having identical amplitudes and uniformly-spaced phases in terms of their radiated fields in the direction of ($\theta = 45°$, $\phi = 0°$) (($\theta = 45°$, $\phi = 180°$)). The overall radiations in these two directions are schematically depicted in (e) and (f) with each black arrow representing one radiation component.

2.2. Plasmonic phased antenna arrays

With the help of Fig. 3, the distributions of the amplitude and phase in an antenna array can be precisely designed. In Figs. 3(a) and 3(b), five nanorods (marked by the red circles) are picked out to form a constructive interference in the direction of ($\theta = 45°$, $\phi = 0°$) and a destructive interference in the direction of ($\theta = 45°$, $\phi = 180°$) (see Fig. 3(e)) simultaneously, which converts the saddle-like radiation pattern of Fig. 1(d) to a unidirectional one exhibited in Fig. 4(d). The phase differences ($\Delta\varphi$, defined in Fig. 3(b)) and the spacing between nanorod pairs (d defined in Fig. 3(e)) obey the following relationships:

$$(n_{\text{eff}} - n_{\text{SiO}_2} \sin\theta)\frac{2\pi}{\lambda}d + \Delta\varphi = 0, \tag{2a}$$

$$(n_{\text{eff}} + n_{\text{SiO}_2} \sin\theta)\frac{2\pi}{\lambda}d + \Delta\varphi = \frac{2\pi}{N}, \tag{2b}$$

where $n_{\text{eff}} = 1.805$ (from Fig. 1(b)), $n_{\text{SiO}_2} = 1.444$, and $N = 5$. In addition, $d \approx 150$ nm and $\Delta\varphi \approx -27.6°$ are derived. In deducing Eq. (2), a hypothesis that the radiated fields in the two directions of ($\theta = 45°$, $\phi = 0°$) and ($\theta = 45°$, $\phi = 180°$) from each nanorod pair are identical is used. This hypothesis ignores the phase retardation accumulated in each nanorod pair and is well supported by the similarity between Figs. 3(a), 3(b) and Figs. 3(c), 3(d).

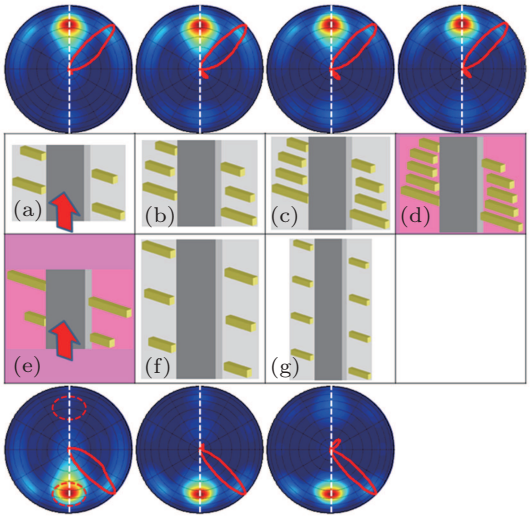


Fig. 4. (color online) Geometries and 3D radiation patterns of the plasmonic phased antenna arrays with $N = 2, 3, 4, 5$ ((a)–(d), Eqs. (2)) and $N' = 2, 3, 4$ ((e)–(g), Eqs. (3)) excited by a silicon waveguide.

Using similar technique, unidirectional emissions can also be obtained in the direction of ($\theta = 45°$, $\phi = 180°$). In Figs. 3(c) and 3(d), two nanorod pairs are selected out to compose a phased antenna array, and generate the radiation pattern shown in Fig. 4(e). The phase difference $\Delta\varphi'$ and the spacing between nanorod pairs d' obey

$$(n_{\text{eff}} - n_{\text{SiO}_2} \sin\theta)\frac{2\pi}{\lambda}d' + \Delta\phi' = \frac{2\pi}{N'}, \tag{3a}$$

$$(n_{\text{eff}} + n_{\text{SiO}_2} \sin\theta)\frac{2\pi}{\lambda}d' + \Delta\phi' = 2\pi, \tag{3b}$$

where $d' \approx 380$ nm, $\Delta\varphi' \approx 111°$, and $N' = 2$.

Figure 4 plots all unidirectional plasmonic phased antenna arrays composed according to Eqs. (2) and (3). The numbers of the nanorod pairs, $N = 2$, 3, 4, 5 and $N' = 2$, 3, 4, are limited by the finite tuning range of the phase of the radiated field (see Figs. 3(b) and 3(d)). In Ref. [22], the authors realized full 2π phase tunability by using a cross polarization configuration, whereas in our case, this tuning range is limited by $\pi/2 + \tan^{-1}(2Q)$ according to Eq. 1(b).

As an example, we analyze in detail the radiation pattern in Fig. 4(e). The reduction of the transmission of the guided wave (9.9%) consists of the metal dissipation (1.6%) and the light emission (8.3%). The emission directionality is thus accompanied by the raise of the cost–effectiveness ratio (∼1/5). In addition, as expected, most of the light emission (73%) enters the substrate side and 0.8% (27%) goes into the angular cone with the central direction of ($\theta = 45°$, $\phi = 0°/180°$) and the half angle of 15°. This gives rise to a large forward-backward contrast ratio (15 dB) and a large antenna directivity (12 dB), defined as the ratio of the maximum radiation intensity in one direction to the average radiation intensity over the full solid angles in the substrate side. In comparison to the directivity of an infinitesimal dipole (1.8 dB), the emission directionality of the plasmonic phased antenna array is significant. Remember that, in the above design process, the mutual couplings between nanorod pairs and the back reactions from the antennae to the guided wave are both ignored. The unidirectional patterns demonstrated in Fig. 4 corroborate these hypotheses.

Before ending this section, we compare our plasmonic phased antenna array with its non-plasmonic counterpart. Figure 5 plots the radiation patterns of these two devices with $N = 2$. The non-plasmonic antenna array consists of two silicon nanorod pairs. This manifests that the plasmonic phased antenna array has the merits of small footprints (0.46 μm versus 2.06 μm in terms of the total lengths) and no high-order diffractions. Without resonant characteristics, non-plasmonic antenna arrays constitute the phase coherence between elements across multiples of 2π, whereas the plasmonic antenna array achieves this within 2π. Moreover, from the viewpoint of practical applications, the high-order diffractive radiations will cause waste and signal crosstalk. The pie charts in Fig. 5 show the distribution of the light energy: the left one in the guided wave (blue), dissipated in the metal (orange), radiated to the air (gray), to the substrate (green), and to the angular cone marked by the dashed circle (red). The plasmonic phased antenna array wins its non-plasmonic counterpart in terms of not only the total light emissions but also the proportion of the useful emission.

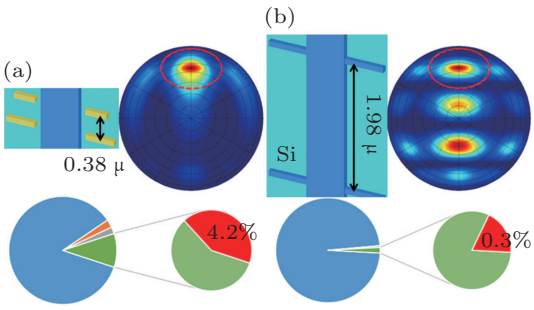


Fig. 5. (color online) Geometry, radiation pattern, and energy's pie chart of (a) a gold antenna arrays and (b) a Si antenna array excited by a Si waveguide. For (a), all the geometrical parameters are the same as Fig. 4(a). For (b), $l = 620$ nm and $s = 0$ nm.

3. Photonic circuits decorated with plasmonic phased antenna arrays

The merits of the plasmonic phased antenna arrays discussed in the last section, i.e., the size compactness and the device effectiveness, are valuable in applications of photonic integrations. As pointed out in Ref. [21], the combination of plasmonic antennae and dielectric waveguides allows one to have both strong optical effects and low-loss light transportations. In the following, we address how optical functions can be engineered in such plasmonic-dielectric hybrid circuits, which have good scalability and can be fabricated by using contemporary lithography technologies.

3.1. Far-field radiations from photonic circuits

Adjusting the orientations of the hybrid waveguide segments and connecting them together provide a convenient method to control the direction and the polarization of the far-field radiation. Figure 6 plots the radiation patterns from a

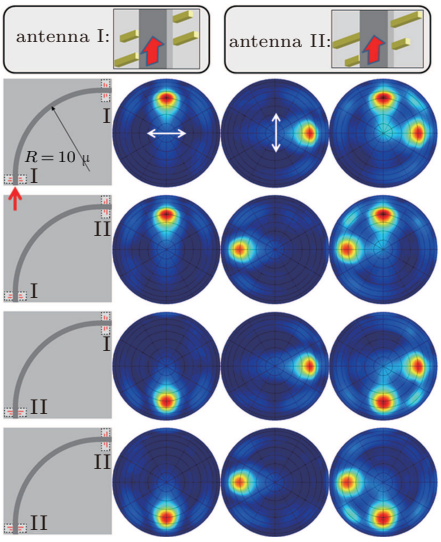


Fig. 6. (color online) Geometries and radiation patterns of a right-angle waveguide bend with the input and output sections decorated with plasmonic phased antenna arrays. The left, middle, and right columns are, respectively, the radiation patterns in the transverse, longitudinal, and both two polarizations. The white arrows represent the polarization directions. The color scales used in all plots are identical.

right-angle waveguide bend with the radius of 10 μm. The segments before and after the bend are the unidirectionally radiative hybrid waveguides. The plasmonic phased antenna arrays of type I and type II corresponding to Figs. 4(a) and 4(e) respectively are used. The FDTD simulations reveal that the overall radiations are mainly from the two subwavelength hybrid waveguide segments and the contributions from other parts can be ignored.

3.2. Wireless light transportations in a layered structure

Exploiting the control capability of the hybrid waveguides with regard to the far-field radiation exhibited in Fig. 6, we envision wireless light transportation between two photonic circuits.

Figure 7(a) depicts a 2-micron-thick silica slab and two parallel silicon waveguides lying on the opposite surfaces of this slab. When light travels through the left waveguide, the plasmonic phased antenna array consisting of five gold nanorod pairs radiates light to the forwardly tilting direction, where another phased antenna array receives and couples the light into the right waveguide. Figure 7(b) shows a peak transmission ($\sim 2.2\%$ with regard to the input power) at the position where the longitudinal distance between two antenna arrays, D, equals to 1.75 μm, agreeing well with the prediction from the radiation pattern (the inset in Fig. 7(a)). Taking into account the fact that the straight-line distance between the two antenna arrays stays in the Fraunhofer far-field range, $2.7\ \mu\text{m} > 2n_{\text{SiO}_2}(0.6\ \mu\text{m})^2/\lambda = 0.67\ \mu\text{m}$, the light transportation should be mediated by radiation, not by near-field coupling. Here, 0.6 μm is the length of the phased antenna array in the longitudinal direction. We further check the modal indices of the even and odd guided modes ($n_e = 1.8057$ and $n_o = 1.8056$) of the two parallel silicon waveguides depicted in Fig. 7(a). The beating length, $\lambda/(n_e - n_o) \approx 15$ mm, is four orders of magnitude greater than the length of the whole device, ruling out the possibility of evanescent coupling between silicon waveguides.

Modifying the configuration in Fig. 7, figure 8 proposes an optical routing structure consisting of one bus (the dark black line) and two branch (the light black ones) photonic wires separated in vertical direction by a 1-micron-thick silica slab. The guided light in the bus photonic wire is delivered to port 1 and port 4 of the two branch wires via the two pairs of plasmonic phased antenna arrays. The functionality of this device is determined by the orientations of the photonic circuits, and the size compactness is due to the adoption of the plasmonic phased antenna arrays. In Fig. 8, the arc radii of the branch photonic wires are 5 μm, which could be further shrunk.[33]

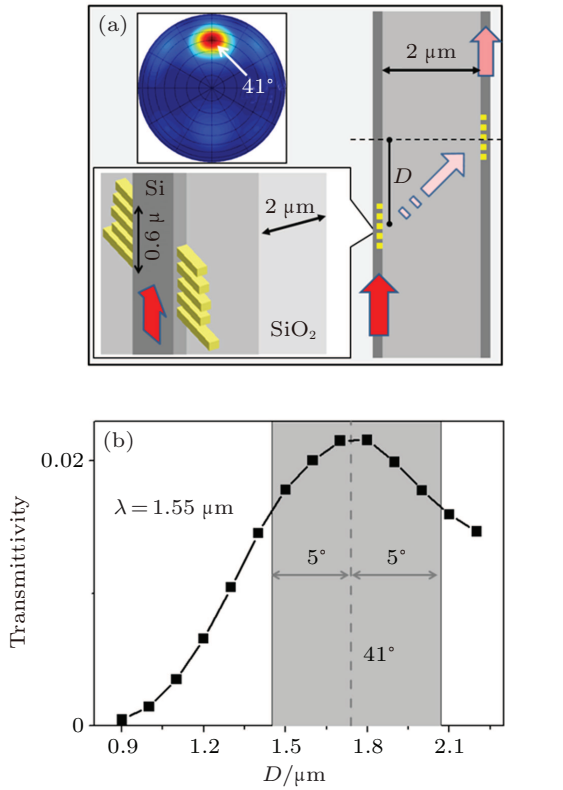


Fig. 7. (color online) (a) Schematic of wireless light transportation from one silicon waveguide to the other by using plasmonic phased antenna arrays. The parameters of the antenna arrays are respectively l = 490/345/350/330/300 nm, s = 0/10/20/10/5 nm, and d = 150 nm. (b) Transmittivity across the two waveguides versus the longitudinal distance D (denoted in (a)).

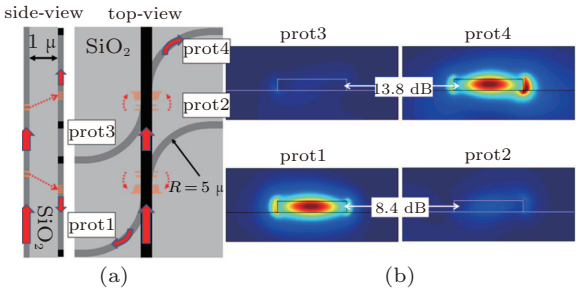


Fig. 8. (color online) (a) Side-view and top-view of a wireless optical router. The light in the bus photonic wire is partly delivered to port 1 and port 4 of the two branch photonic wires (following the red arrows). (b) Simulated intensity profiles at the four ports of the branch wires. The contrast ratio of the intensity at port 1 (port 4) to that at port 2 (port 3) is 8.4 dB (13.8 dB). Identical color scales are used in all the four plots.

4. Discussion and conclusions

In this study, the emission directionality of an optical antenna is aimed as the only target. As pointed out in Ref. [34], emission directionality and emission enhancement are hard to be achieved simultaneously. In a directional antenna, the enhanced emission in one direction is usually accompanied by even stronger suppression to the emissions in other directions. Being aware of this, we set the emission enhancement in our plasmonic phased antenna arrays as the secondary target. Fortunately, there are plentiful methods to enhance the field amplitude inside a dielectric waveguide, e.g., via cavity enhance-

ment effects.

Second, we restrain our studies in monochromatic situations. Broadband properties of the plasmonic phased antenna arrays, which are very important in ultrafast optical applications, have recently been reported by Sidiropoulos *et al.*[35] The dispersion of this device is very low.

Third, wireless light transportations via nano-antennae have already been suggested to replace nanoscale optical waveguides on chips.[25] Our work points out that such applications should be implemented in a layered structure, which stimulates people to design and fabricate integrated photonic networks with 3D configuration.

In summary, numerical investigations have been carried out to exhibit far-field radiation properties of the plasmonic phased antenna arrays in context of dielectric photonic circuits. One pair of gold nanorods laterally excited by a silicon waveguide are first studied. The resonant nature, which is mainly embodied in its Q factor, along with the independent amplitude/phase adjusting freedom, which is realized by tuning two geometrical parameters, enable us to easily and precisely design the field distribution across an antenna array. The plasmonic phased antenna arrays exhibit unidirectional emissions with typical forwardbackward contrast ratio of 15 dB and antenna directivity of 12 dB together with size compactness. Then, by varying the orientations of the antenna array decorated waveguide segments and connecting them together, wireless light transportations between photonic circuits and optical routing functions are proposed in a layered structure, which may be applied in future high-density photonic integrations.

References

[1] Maier S A 2007 *Plasmonics: Fundamentals and Applications* (New York: Springer)
[2] Xu H, Aizpurua J, Kall M and Apell P 2000 *Phys. Rev. E* **62** 4318
[3] Farahani J N, Pohl D W, Eisler H J and Hecht B 2005 *Phys. Rev. Lett.* **95** 017402
[4] Kuhn S, Hakanson U, Rogobete L and Sandoghdar V 2006 *Phys. Rev. Lett.* **97** 017402
[5] Kim S, Jin J, Kim Y J, Park I Y, Kim Y and Kim S W 2008 *Nature* **453** 757
[6] Oulton R F, Sorger V J, Genov D A, Pile D F P and Zhang X 2008 *Nat. Photon.* **2** 496
[7] Barnes W L, Dereux A and Ebbesen T W 2003 *Nature* **424** 824
[8] Tang L, Kocabas S E, Latif S, Okyay A, Ly-Gagnon D S, Saraswat K C and Miller D A B 2008 *Nat. Photon.* **2** 226
[9] Atwater H A and Polman A 2010 *Nat. Mater.* **9** 205
[10] Taminiau T H, Moerland R J, Segerink F B, Kuipers L and van Hulst N F 2007 *Nano Lett.* **7** 28
[11] Chang D E, Sorensen A S, Demier E A and Lukin M D 2007 *Nat. Phys.* **3** 807
[12] van Zanten T S, Lopez-Busquets M J and Garcia-Parajo M F 2010 *Small* **6** 270
[13] Pakizeh T and Kall M 2009 *Nano Lett.* **9** 2343
[14] Evlyukhin A B, Bozhevolnyi S I, Pors A, Nielsen M G, Radko I P, Willatzen M and Albrektsen O 2010 *Nano Lett.* **10** 4571
[15] Shegai T, Chen S, Miljkovic V D, Zengin G, Johansson P and Kall M 2011 *Nat. Commun.* **2** 481
[16] Curto A G, Volpe G, Taminiau T H, Kreuzer M P, Quidant R and van Hulst N F 2010 *Science* **329** 930
[17] Kosako T, Kadoya Y and Hofmann H F 2010 *Nat. Photon.* **4** 312
[18] Balanis C A 2005 *Antenna Theory: Analysis and Design* (3rd edn.) (New Jersey: John Wiley & Sons)
[19] Sugita T, Maeda S, Hofmann H F and Kadoya Y 2013 *Proceeding of the Conference on Lasers and Electro-Optics* (QF2A.6)
[20] Maier S A Brongersma M L, Kik P G, Meltzer S, Requicha A A G and Atwater H A 2001 *Adv. Mater.* **13** 1501
[21] Arango F B, Kwadrin A and Koenderink A F 2012 *ACS Nano* **6** 10156
[22] Yu N, Genevet P, Kats M A, Aieta F, Tetienne J P, Capasso F and Gaburro Z 2011 *Science* **334** 333
[23] Shadrivov I V, Kapitanova P V, Maslovski S I and Kivshar Y S 2012 *Phys. Rev. Lett.* **109** 083902
[24] Lipson M 2005 *J. Lightwave Technol.* **23** 4222
[25] Alu A and Engheta N 2010 *Phys. Rev. Lett.* **104** 213902
[26] Palik E D 1998 *Handbook of Optical Constants of Solid* (Amsterdam: Elsevier)
[27] Ding W, Bachelot R, de Lamaestre R E, Macias D, Baudrion A L and Royer P 2009 *Opt. Express* **17** 21228
[28] Jalali B and Fathpour S 2006 *J. Lightwave Technol.* **24** 4600
[29] Huang C, Bouhelier A, des Francs G C, Bruyant A, Guenot A, Finot E, Weeber J C and Dereux A 2008 *Phys. Rev. B* **78** 155407
[30] Lieb M A, Zavislan J M and Novotny L 2004 *J. Opt. Soc. Am. B* **21** 1210
[31] Engheta N, Salandrino A and Alu A 2005 *Phys. Rev. Lett.* **95** 095504
[32] Lerosey G, Pile D F P, Matheu P, Bartal G and Zhang X 2009 *Nano Lett.* **9** 327
[33] Xu Q, Fattal D and Beausoleil R G 2008 *Opt. Express* **16** 4309
[34] Hofmann H F, Kosako T and Kadoya Y 2007 *New J. Phys.* **9** 217
[35] Sidiropoulos T P H, Maier S A and Oulton R F 2012 *Opt. Express* **20** 12359